

Supplemental material

Table-of-contents:

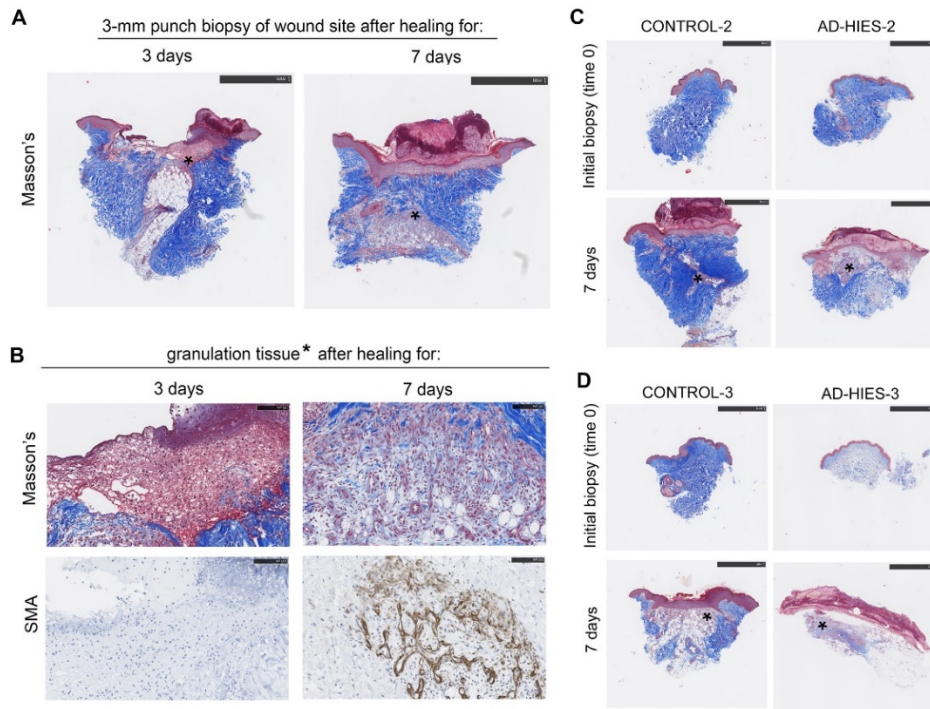
(use blue links and/or bookmarks for easier navigation)

| 1. Supplemental Figures | Page |
|--|-------------|
| Supplemental Figure 1 (related to Figure 1). Analysis of skin wound healing in AD-HIES patients using wound healing model based on repeated skin biopsies..... | 3 |
| Supplemental Figure 2 . TNF α activates STAT3 in primary human skin fibroblasts by an autocrine mechanism mediated through IL-6 receptor. | 4 |
| Supplemental Figure 3 (related to Figure 2). Map of the Extracellular Matrix (ECM) Remodeling pathway, the top enriched pathway in genes that are differentially expressed in AD-HIES vs CT skin fibroblasts..... | 5 |
| Supplemental Figure 4 (related to Figure 2). RNA-Seq analysis of signaling pathways dysregulated in AD-HIES HUVECs..... | 6 |
| Supplemental Figure 5 (related to Figure 2). Verification of changes identified by RNA-seq in the expression of genes related to angiogenesis and ECM remodeling in AD-HIES skin fibroblasts, and of the STAT3 dependence of those changes..... | 7 |
| Supplemental Figure 6 (related to Figure 3). AD-HIES iPSC-derived teratomas are composed of cells and structures derived from all three germ layers consistent with normal pluripotency potential of AD-HIES iPSCs but display severe growth retardation. The growth deficiency can be rescued by co-injection of control, but not AD-HIES skin fibroblasts..... | 8 |
| Supplemental Figure 7 (related to Figure 3). Analysis of teratoma vascularization based on staining for endothelial cell marker CD31..... | 9 |
| Supplemental Figure 8 (related to Figure 4). Deficient HIF1 α signaling in AD-HIES skin fibroblasts both at transcriptional and protein stabilization levels (supporting experiments for Figure 4)..... | 10 |
| Supplemental Figure 9 (related to Figure 4). STAT3 binding sites in promoter of <i>HIF1A</i> gene..... | 11 |
| Supplemental Figure 10 (related to Figure 4). Verification of the STAT3-dependency of HIF1 α expression and stabilization deficiency observed in AD-HIES cells..... | 12 |
| Supplemental Figure 11 (related to Figure 5). Analysis of ECM composition in coronary arteries (CA) of AD-HIES patients..... | 13 |
| Supplemental Figure 12 (related to Figure 7). Analysis of mouse model of AD-HIES..... | 14 |
| Supplemental Figure 13 (related to Figure 7). Dimethyl fumarate (DMF) improves Th17 generation from naïve cells of AD-HIES patients..... | 15 |
| 2. Supplemental Movies | |
| Supplemental Movie 1 (related to Figure 7). 3D reconstruction of coronary arterial network of AD-HIES mouse..... | 16 |
| Supplemental Movie 2 (related to Figure 7). 3D reconstruction of coronary arterial network of WT mouse..... | 16 |

3. Supplemental Tables

| | |
|---|-------|
| Supplemental Table 1 . Information about AD-HIES patients and controls used in the study. | 17 |
| Supplemental Table 2 (related to Figure 2). RNA-Seq analysis of genes and signaling pathways that are affected by AD-HIES STAT3 mutations. | 17 |
| Supplemental Table 3 . Primer sequences that were used in the study..... | 18 |
| 4. Supplemental methods | 19-29 |
| 5. References | 30 |

Supplemental Figures



Supplemental Figure 1 (related to Figure 1). Analysis of skin wound healing in AD-HIES patients using wound healing model based on repeated skin biopsies.

3 AD-HIES patients and 3 healthy volunteers matched by age, gender and race underwent wound healing study procedure as described on Figure 1A. Skin wound was created using 2-mm skin punch biopsy tool by removing 2 mm diameter cylindrical core of tissue excised to the depth of the deep dermis/dermal subcutaneous junction (including epidermis, dermis and superficial subcutis). Three or seven days later, 3-mm skin punch biopsy of the wound site was performed, tissue was fixed in neutral buffered formalin and routinely processed, embedded into paraffin and the wound healing process was analyzed by routine histology, special stains, and immunohistochemistry.

(A, B) Day seven represent optimal time point for analysis of fibroplasia and angiogenesis. Result for control volunteer is shown:

(A) Representative images of punch skin biopsies, sectioned and stained with Masson's Trichrome stain, for initial analysis of extracellular matrix restoration and epidermal re-epithelialization during wound healing. By day 7, wound is completely covered by newly formed epithelium, large area of wound defect beneath the epithelium is filled with collagen (blue) and active granulation tissue is also present (asterisk). Scale bar = 1mm.

(B) Higher magnification of the areas labeled with asterisks to reveal the structure of active granulation tissue present in wounds at day 3 and 7. *Upper panels:* Masson's stain demonstrating that granulation tissue at day 3 is in inflammatory stage, composed mostly of inflammatory cells and lacking collagen. At day 7, granulation tissue is in proliferative stage, is filled with fibroblasts actively forming new collagen (blue fibers) and contains newly formed blood vessels. *Lower panel:* Staining of the same area as on upper panel for SMA to detect smooth muscle cells in blood vessels walls and active myofibroblasts. The staining demonstrates absence of vascularization and active myofibroblasts in granulation tissue at day 3, and their presence at day 7. Scale bar = 100µm.

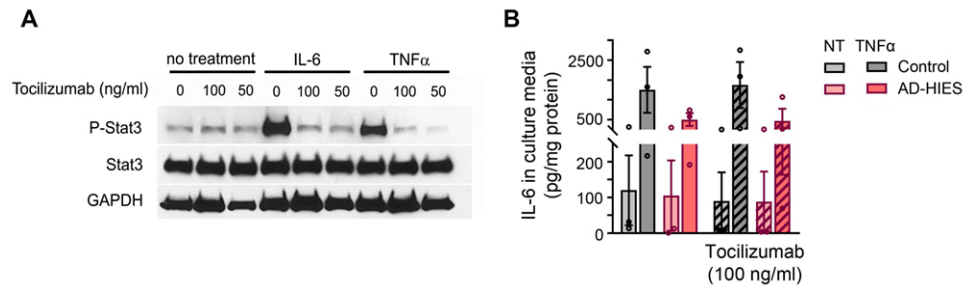
(C, D) Formation and maturation of granulation tissue is delayed in AD-HIES.

Images are shown for 2 AD-HIES patients and their matched controls

(Upper panels) Histology images of Masson's trichrome staining of initial biopsies sections demonstrating normal distribution of collagen fibers and cutaneous structure in undamaged skin;

(Lower panels) Histology images of Masson's trichrome staining of skin tissues after 7 days of healing. Bright blue staining indicates areas with abundant collagen. Red color is seen in areas of early granulation tissue with less collagen (asterisks). AD-HIES sections contain larger areas of immature granulation tissue with less collagen. Scale bar = 1mm. See Figure 1A-E for quantifications and further analysis.

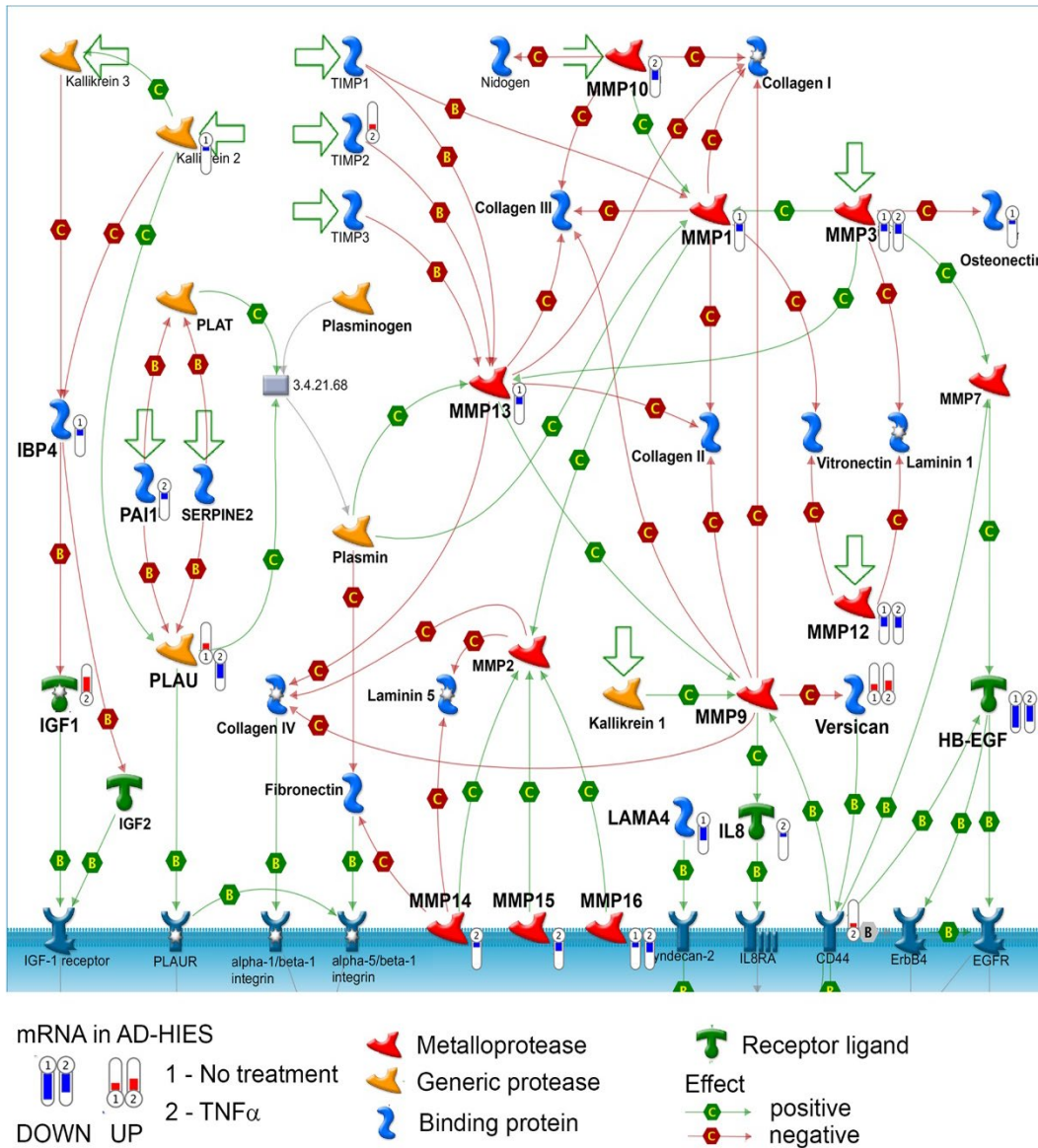
See Supplemental Table 1 for information about patient samples used in these experiments.



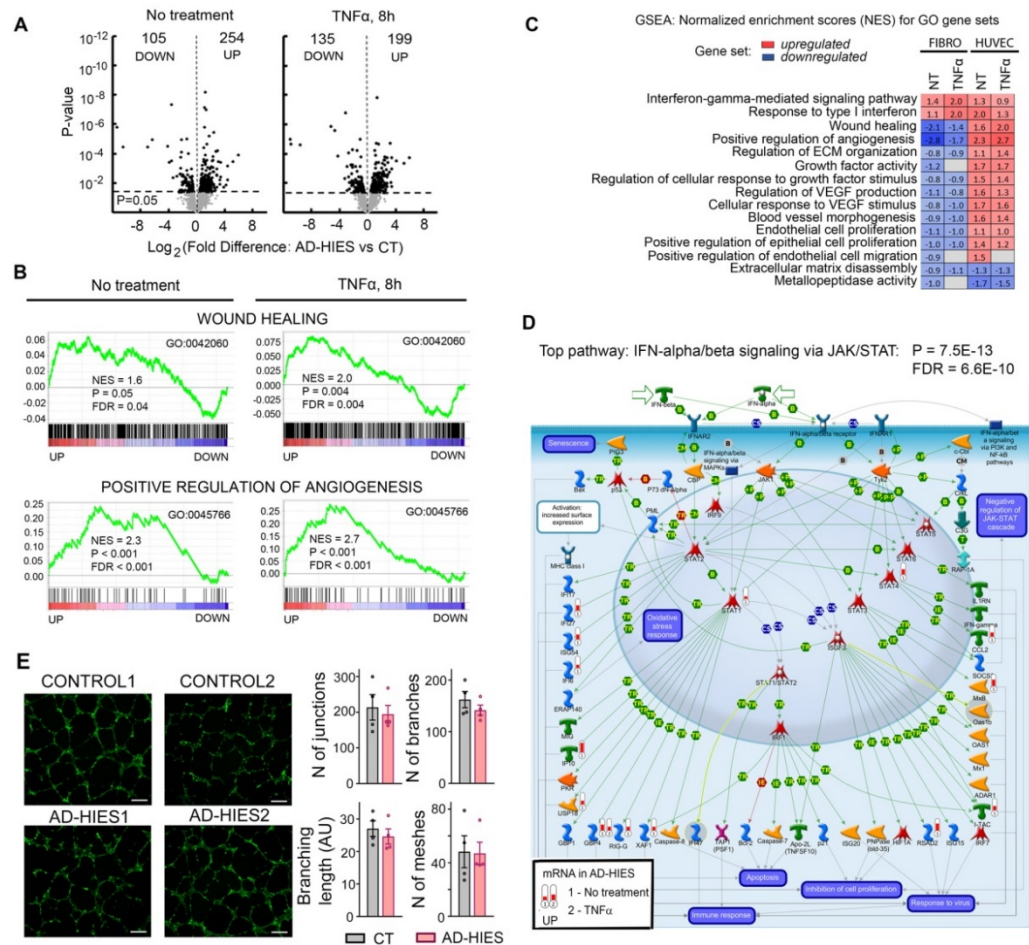
Supplemental Figure 2. Characterization of STAT3 activation by cytokines in primary human skin fibroblasts cell culture model. STAT3 is activated by IL6. TNF α activates STAT3 by an autocrine mechanism mediated through IL-6 receptor.

(A) Normal human skin fibroblasts (BJ, No. CRL-2522, ATCC), cultured as described in the Methods, were pretreated with or without IL-6 receptor blocker Tocilizumab and then exposed to IL-6 (50ng/ml) for 30 min or TNF α (50 ng/ml) for 2h. Phosphorylation of STAT3 at Tyr705 was evaluated by western blot as described in the Methods as a measure of STAT3 activity. Representative western blot image is shown. Blocking of the IL-6 receptor prevents IL-6 and TNF α - induced phosphorylation of STAT3 indicating that the phosphorylation is mediated through the IL-6 receptor.

(B) IL-6 was measured in cell culture media after 8h of TNF treatment. Both control and AD-HIES fibroblasts secrete detectable levels of IL-6 in basal condition and increase the secretion in response to TNF α .



Supplemental Figure 3 (related to Figure 2). Map of the Extracellular Matrix (ECM) Remodeling pathway, the top enriched pathway in genes that are differentially expressed in AD-HIES vs CT skin fibroblasts. Pathway analysis was performed with GeneGo Metacore on differentially expressed genes with p-value = 0.05 cut off. Pathway enrichment statistics: p-value = 1.9E-8; FDR = 5.2E-5.



Supplemental Figure 4 (related to Figure 2). RNA-Seq analysis of signaling pathways dysregulated in AD-HIES HUVECs. Cultured endothelial cells isolated from umbilical cords of 3 babies with AD-HIES STAT3 mutations and from 3 control cords were treated with or without TNF α for 8h and mRNA expression profiles were analyzed by RNA-Seq.

(A) Overview of the differences in mRNA expression in AD-HIES vs control (CT) HUVECs. Expression data are plotted in the form of a Volcano Plot that plots fold difference vs p-value of the difference for each expressed gene.

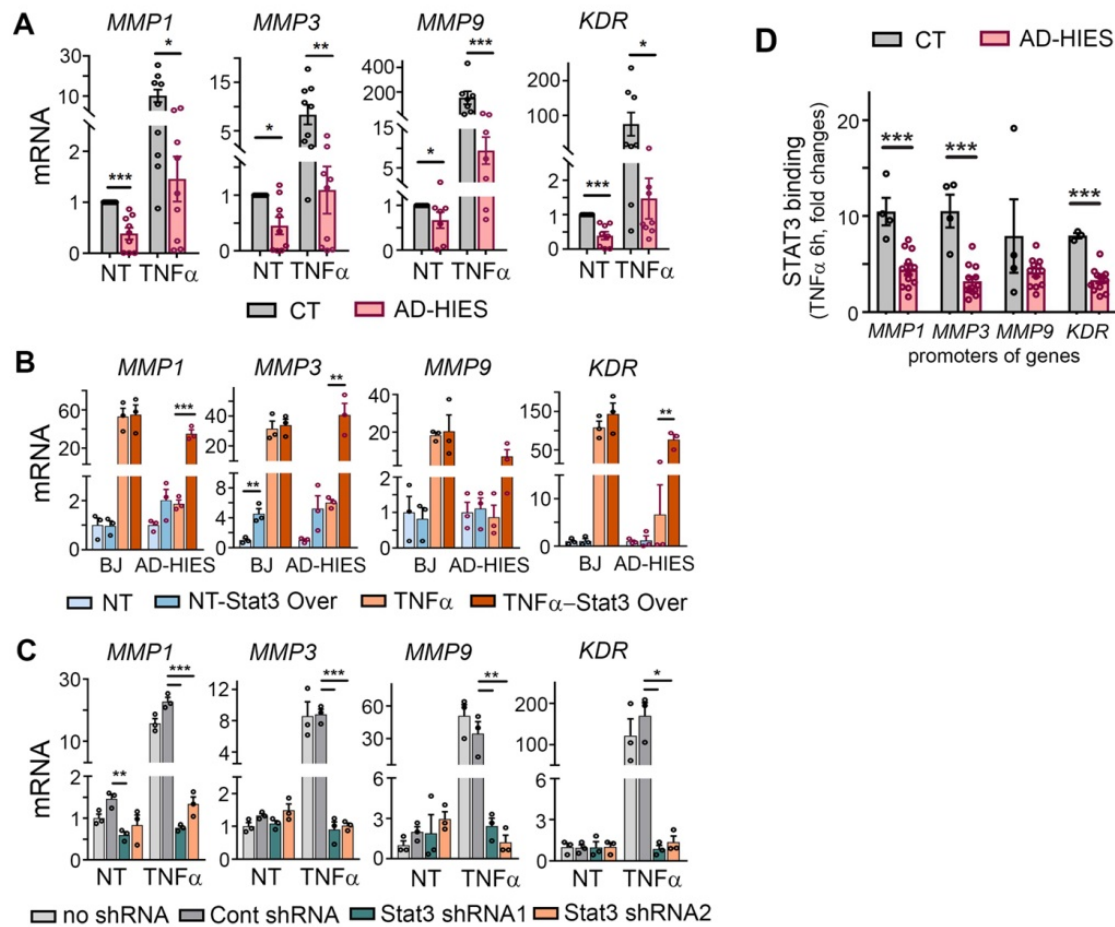
(B, C) Biological processes and pathways related to wound healing, angiogenesis and growth factors signaling are upregulated in AD-HIES HUVECs. Gene set enrichment analysis (GSEA) is performed in Broad Institute software.

(B) Enrichment plots for the Wound Healing gene signature (GO: 0042060) and the Positive Regulation of Angiogenesis gene signature (GO: 0045766) in AD-HIES compared to CT. Opposite to skin fibroblasts (Figure 2), AD-HIES HUVECs demonstrate concordant increase of expression of the genes in these sets

(C) List of biological processes that were analyzed by GSEA in HUVECs to compare expression changes with skin fibroblasts. For each gene set, the name of the biological process is shown on the left. Heat map on the right visualizes normalized enrichment scores (NES) for corresponding gene set for AD-HIES skin fibroblasts and HUVECs.

(D) Map of the Interferon-alpha/beta signaling via Jak/STAT pathway, the top enriched pathway in genes that are differentially expressed in AD-HIES vs CT skin HUVECs. Pathway analysis was performed in Metacore (Clarivate Analytics) on differentially expressed genes with p-value = 0.05 cut off.

(E) Normal angiogenic potential of AD-HIES HUVECs assessed by endothelial cells tube formation assay. Control and AD-HIES HUVECs were cultured on matrigel matrix for 6h (see methods for details) Left panel: Representative images. Cells are stained with Calcein AM Dye (No. 354216, BD Biosciences). Scale bar=200 μ m. Right panels: Quantification of different features of the tubule structures (mean \pm SEM; n=4).



Supplemental Figure 5 (related to Figure 2). Verification of changes identified by RNA-seq in the expression of genes related to angiogenesis and ECM remodeling in AD-HIES skin fibroblasts (SFs), and of the STAT3 dependence of those changes.

Cultured primary skin fibroblasts generated from AD-HIES patients and normal control (CT) volunteers or normal skin BJ fibroblasts were treated with or without TNF α for 8h (NT = no treatment).

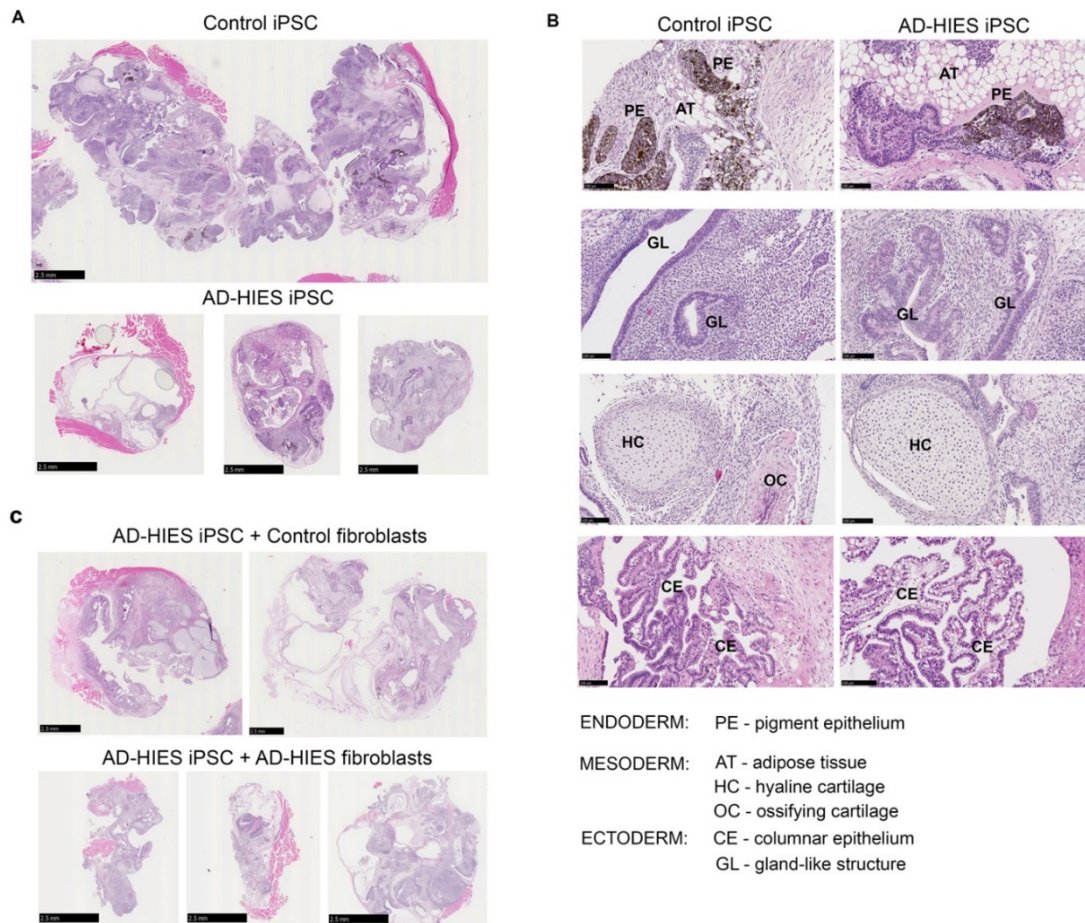
(A) AD-HIES SFs have decreased *MMPs* and *KDR* mRNA expression both in no treatment (NT) condition and after stimulation with TNF α (analyzed by qPCR). The data are plotted as mRNA copy number relative to 18S mRNA and corresponding CT (mean \pm SEM; n=9, *P<0.05; **P<0.01; ***P<0.001, Mann-Whitney Rank Sum Test).

(B) Overexpression of normal STAT3 increases mRNA expression of *MMPs* and *KDR* in AD-HIES SFs.

(C) shRNA -mediated knockdown of STAT3 in normal skin BJ fibroblasts decreases mRNA expression of *MMPs* and *KDR*. In (B) and (C) the data are plotted as mRNA copy number relative to 18S mRNA and NT control (mean \pm SEM; n=3, **P<0.01; ***P<0.001, two tailed, unpaired t test).

(D) Decreased binding of AD-HIES STAT3 to the promoters of *MMPs* and *KDR* genes. Cells were treated or not with 50ng/ml TNF α for 6h. Chromatin Immunoprecipitation (ChIP) was performed as described in methods; STAT3 binding is calculated as fold difference of target fragments number in STAT3 ChIP relative to IgG ChIP and then normalized to the no treatment control (mean \pm SEM, WT: n=4; AD-HIES: n = 12; ***P<0.001, two tailed unpaired t test).

See Supplemental Table 1 for the information about patient cells used for these experiments.

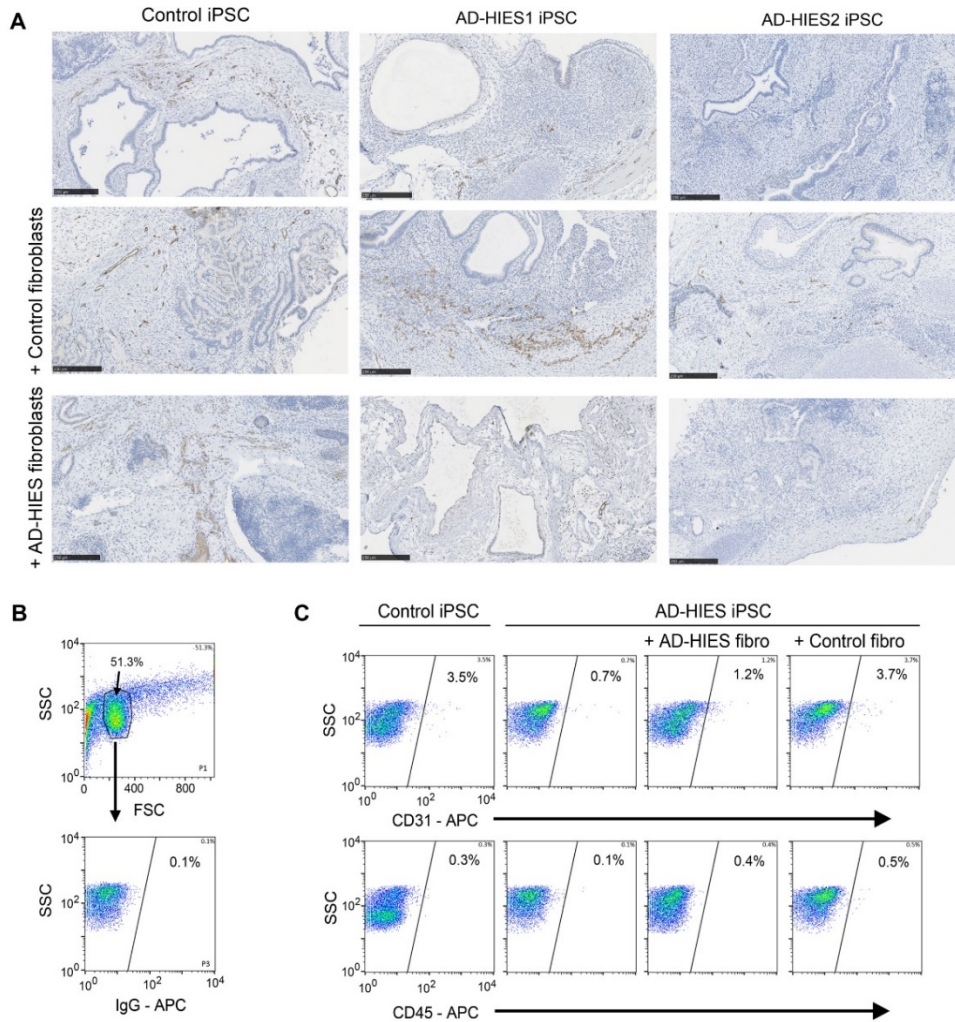


Supplemental Figure 6 (related to Figure 3). AD-HIES iPSC-derived teratomas are composed of cells and structures derived from all three germ layers consistent with normal pluripotency potential of AD-HIES iPSCs but display severe growth retardation. The growth deficiency can be rescued by co-injection of control, but not AD-HIES skin fibroblasts. Control or AD-HIES iPSCs were injected into calf muscle of immunodeficient mice. Teratomas formed in 6-8 weeks were excised for analysis. Teratomas were processed for paraffin blocks and sections and were stained with eosin & hematoxylin to analyze tissue structures.

(A) Representative images of whole teratomas demonstrating much smaller sizes of teratomas derived from AD-HIES iPSCs as compared with control iPSCs. Scale bar = 2.5mm. See also Figure 3D for analysis of teratomas sizes based on weight.

(B) Teratomas derived from both control and AD-HIES iPSC contain structures representing all three germ layers indicating similar differentiation potential. Scale bar = 100 μ m.

(C) AD-HIES iPSC were mixed with Control or AD-HIES fibroblasts and the mixtures were injected into calf muscle of immunodeficient mice. Representative images of whole teratomas are shown. Control but not AD-HIES fibroblasts rescued the growth defect of AD-HIES iPSC-derived teratomas suggesting that they are able to provide a paracrine support for the growth.



Supplemental Figure 7 (related to Figure 3). Analysis of teratoma vascularization based on staining for endothelial cell marker CD31. Control or AD-HIES iPSCs alone or as a mixture with control or AD-HIES fibroblasts were injected into calf muscle of immunodeficient mice.

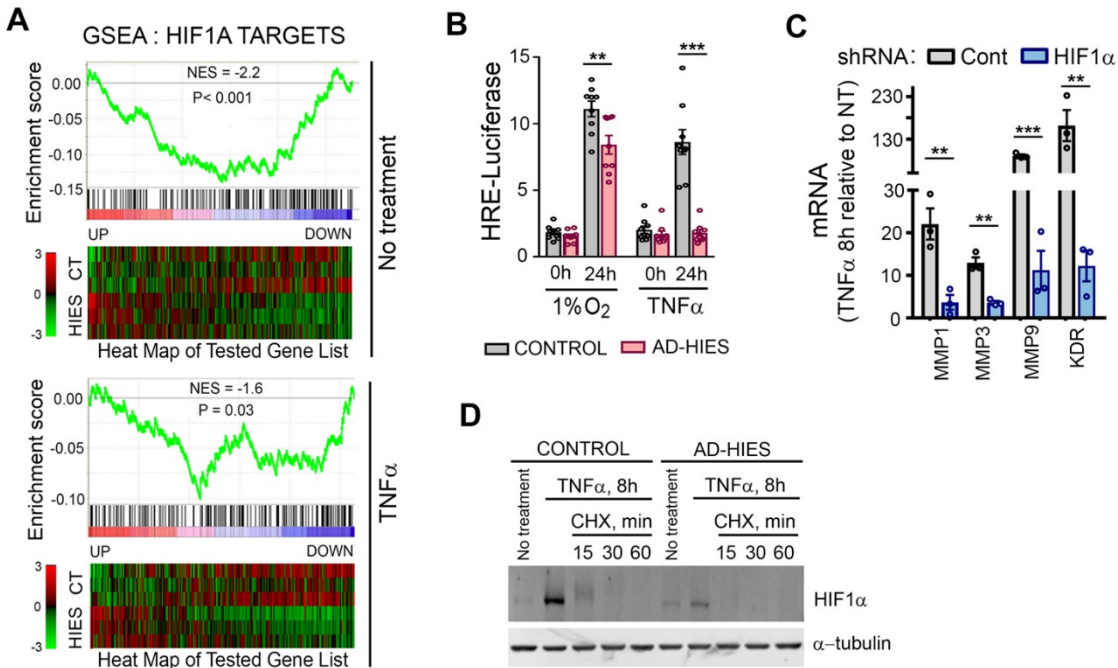
(A) Teratoma tissue sections were immunostained for endothelial cells marker CD31 and distribution and amount of blood vessels was examined. Representative images are shown. Scale bar = 250 μ m. Visual examination of the staining suggests that control iPSC-derived teratomas have more blood vessels that are more evenly distributed throughout the tissue as compared with AD-HIES iPSC-derived teratomas.

(B, C) Quantification of proportion of CD31 positive cells in teratomas by flow cytometry after digestion of the teratomas to single cell suspension followed by staining for CD31. Staining for CD45 was also performed and showed very low positive cell number that is similar in all teratomas. The result excludes the possibility that blood cells that could be positive for CD31 can interfere with the analysis.

(B) Outline of gating strategy. Single cells were selected based on forward vs side scatter plots (upper panel). Gate boundaries for CD31 and CD45 positive cells were set based on IgG control staining (lower panel).

(C) Representative cytograms demonstrating results of the analysis. See Figure 3D for final graph and statistics.

Conclusion: co-injection of AD-HIES iPSC with control but not AD-HIES fibroblasts increases density of blood vessels in teratoma tissue consistent with notion that control fibroblasts are able to provide paracrine support that stimulates angiogenesis and teratoma growth while AD-HIES fibroblasts are deficient in production of the pro-angiogenic factors.



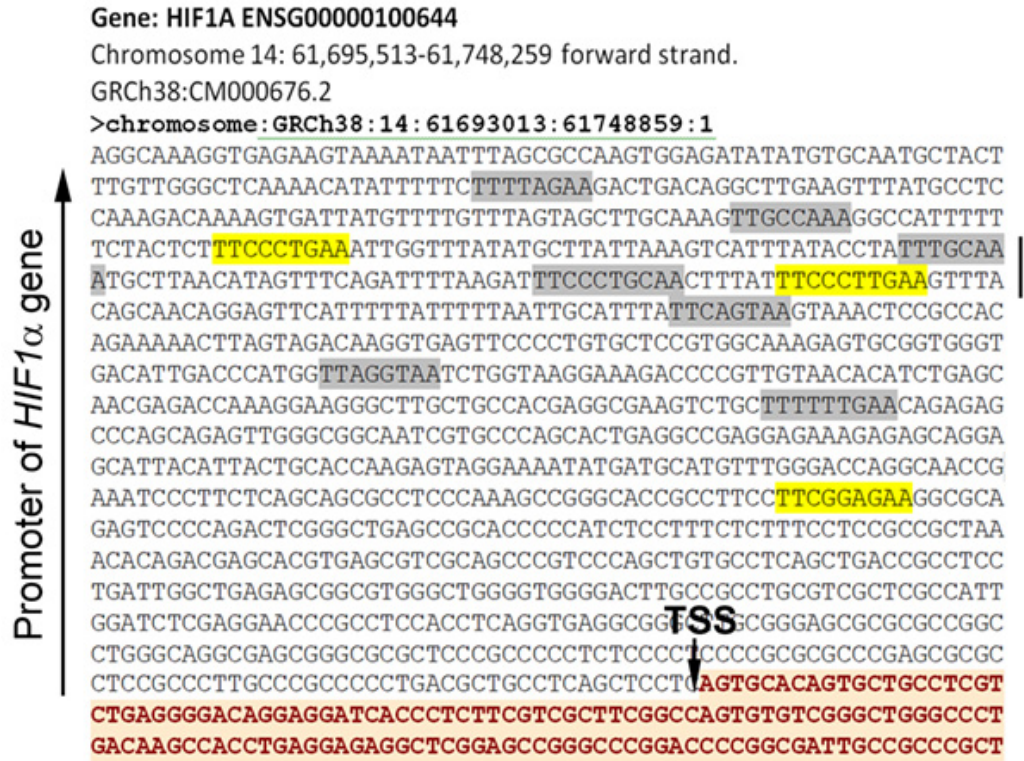
Supplemental Figure 8 (related to Figure 4). Deficient HIF1 α signaling in AD-HIES skin fibroblasts both at transcriptional and protein stabilization levels (supporting experiments for Figure 4).

(A) Gene Set Enrichment Analysis of RNA-Seq data identifies a concordant decreased expression of HIF1 α transcriptional targets in AD-HIES fibroblasts both in basal condition and after treatment with TNF α . See Figure 2 legend and methods for details of the treatments and analysis.

(B) In AD-HIES fibroblasts, transcriptional activity of HIF1 α is increased to smaller degree in response to hypoxia and does not increase in response to TNF α . A luciferase reporter construct containing three hypoxia response elements (HRE) was transfected into fibroblasts and Luciferase expression was measured after treatment with 1% O₂ or TNF α for 24h.

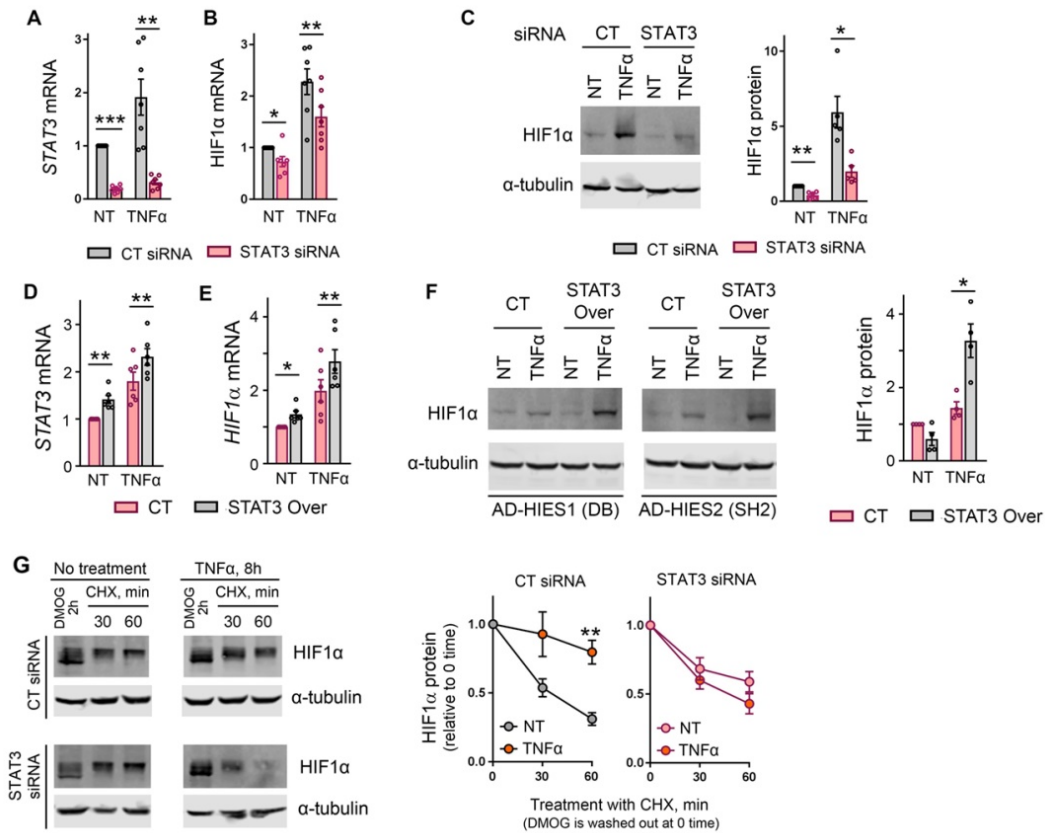
(C) shRNA -mediated knockdown of HIF1A in normal skin BJ fibroblasts decreases mRNA expression of *MMPs* and *KDR*. (mean \pm SEM; n=3, **P<0.01; ***P<0.001; two tailed unpaired t test).

(D) Preliminary experiment estimating stability of HIF1 α protein in human skin fibroblasts (related to Figure 4F-H). To measure rate of HIF1 α protein degradation, de-novo protein synthesis was inhibited with cycloheximide (CHX). Representative Western blot showing fast decrease of HIF1 α protein to undetectable level after addition of CHX, consistent with its low abundance and very short half-life.



Supplemental Figure 9 (related to Figure 4). STAT3 binding sites in promoter of *HIF1A* gene.

Promoter sequence upstream of transcription start site (TSS) of human *HIF1A* gene was retrieved using Ensembl genome browser. Many potential binding sites for STAT3 are found in the promoter region, both canonical (TTC(N)₂₋₄GAA, highlighted in yellow) and less stringent (TT(N)₄₋₆AA, highlighted in grey). The primer pair for STAT3 Chromatin precipitation (ChIP) were designed using the Primer-BLAST tool (<http://www.ncbi.nlm.nih.gov/tools/primer-blast/>) to span these binding sites as shown. See Figure 4D for the ChIP results and Supplemental Table 3 for the primers sequences. Specificities of the primers were verified by analysis of melting curves of the PCR products obtained at the end of SYBR Green qPCR reaction. They produced a single peak.



Supplemental Figure 10 (related to Figure 4). Verification of the STAT3-dependency of HIF1 α expression and stabilization deficiency observed in AD-HIES cells.

(A-C) *siRNA* -mediated knockdown of *STAT3* in control skin fibroblasts decreases mRNA and protein expression of *HIF1 α* . Skin fibroblasts from control volunteers were transfected with *STAT3* siRNA for 24h, incubated in serum free media for 16h and treated or not (NT) with 50ng/ml TNF α for 8h.

(A) *STAT3* mRNA: qPCR and

(B) *HIF1 α* mRNA: qPCR; (mean \pm SEM; n=7, *P<0.05; **P<0.01; ***P<0.001, two tailed, paired t test).

(C) *HIF1 α* protein. *Left panel*: representative Western blot images; *Right panel*: Quantification by densitometry (mean \pm SEM; n=5, *P<0.05, **P<0.01, two tailed, paired t test).

(D-F) Overexpression of normal *STAT3* in AD-HIES skin fibroblasts increases mRNA and protein expression of *HIF1 α* .

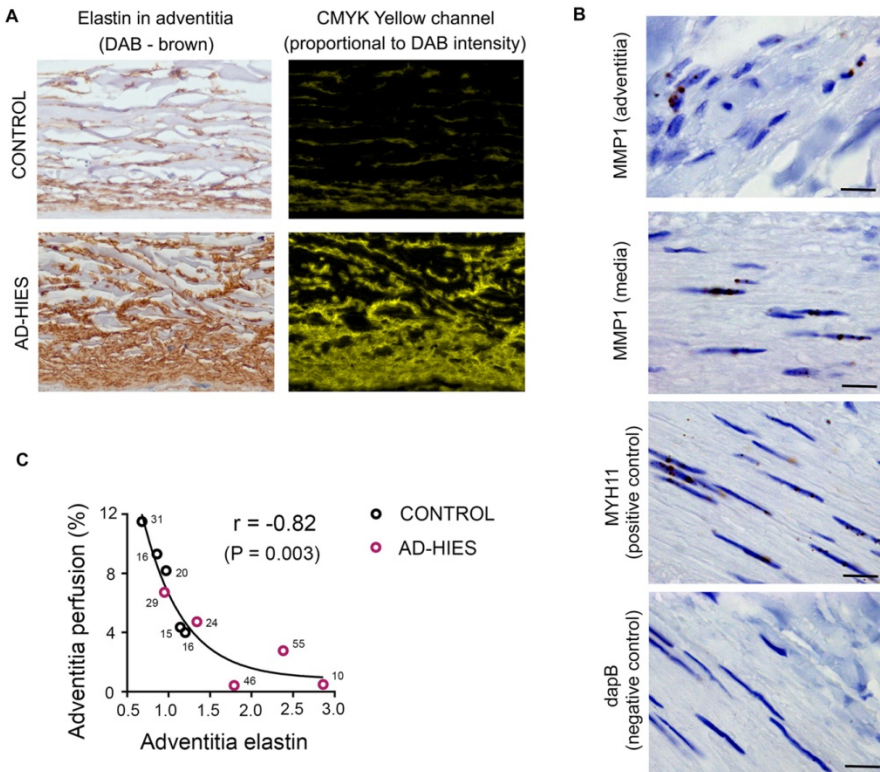
(D) *STAT3* mRNA: qPCR and

(E) *HIF1 α* mRNA: qPCR; (mean \pm SEM; n=6, *P<0.05; **P<0.01; two tailed, paired t test).

(F) *HIF1 α* protein. *Left panel*: representative Western blot images; *Right panel*: Quantification by densitometry (mean \pm SEM; n=4, *P<0.05, **P<0.01, two tailed, paired t test). In A), B), D) and E), the data are plotted as mRNA copy number relative to 18S RNA and NT control.

(G) *siRNA* -mediated knockdown of *STAT3* in control skin fibroblasts prevents TNF α -induced stabilization of *HIF1 α* protein. Skin fibroblasts from control volunteers were transfected with *STAT3* siRNA for 24h, incubated in serum free media for 16h and treated or not (NT) with 50ng/ml TNF α for 8h. To measure rate of *HIF1 α* protein degradation, de-novo protein synthesis was inhibited with cycloheximide (CHX). To increase level of *HIF1 α* , cells were treated for 2h with competitive inhibitor of PHDs dimethylxallylglycine (DMOG) that was washed out before addition of CHX. *Left panels*: Representative Western blot images showing dynamics of *HIF1 α* decrease after addition of CHX. *Right panels*: Quantification of western blots by densitometry (mean \pm SEM; n=6, **P<0.01 relative to NT; two tailed unpaired t test).

See Supplemental Table 1 for the information about patient cells used for these experiments.

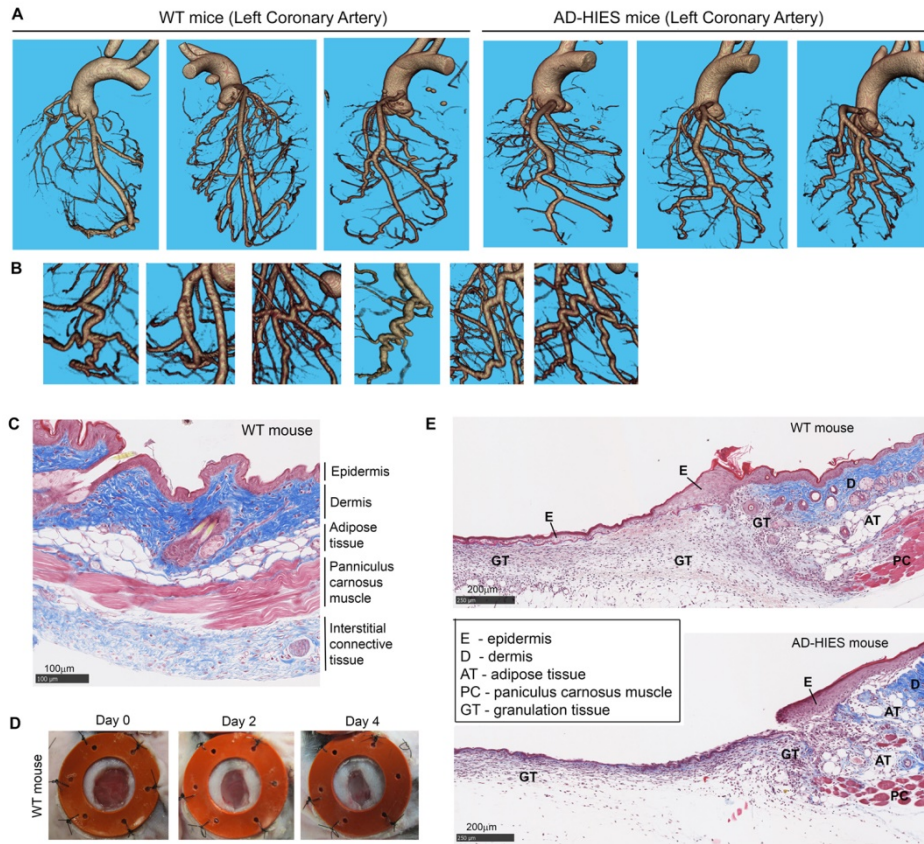


Supplemental Figure 11 (related to Figure 5). Analysis of ECM composition in coronary arteries (CA) of AD-HIES patients

(A) Representative examples of yellow channel extraction from images made using CMYK color model of coronary arteries sections stained for elastin using diaminobenzidine (DAB) chromogen and counterstained with hematoxylin. Left panels: Original images; Right panels: Images of extracted CMYK yellow channel. The pattern and intensity of the signal in the CMYK yellow channel (right panels) corresponds in pattern and intensity to the brown DAB staining of elastin (left panels). Also see Methods and Figure 5F for full description and results of the quantification for elastin, collagen I, collagen IV and laminin in coronary arteries from control and AD-HIES patients.

(B) RNAscope detection of MMP1 mRNA on human coronary arteries sections. Chromogenic staining (DAB – brown) of coronary arteries sections with probes against MMP1 mRNA, MYH11 as positive control expressed in smooth muscle cells and bacterial gene dapB as negative control. Nuclei were counterstained with hematoxylin. Scale bar = 10 μ m. See Figure 5C for quantification results.

(C) Strong correlation between abundance of adventitia elastin and perfusion by vasa vasorum in human coronary arteries (CA). Paraffin section of coronary arteries of control and AD-HIES patients were immunostained for elastin and for CD31 to identify VV vessels in adventitia. Abundance of elastin was measured based on intensity of DAB staining (See Figure 5F and Supplemental Figure 11A for details). Adventitia blood perfusion was measured as % of adventitia area occupied by vasa vasorum (See also Figure 5D for representative images and quantification). For the correlation analysis, all the coronary arteries were analysed together independent on STAT3 mutation status. Strong correlation is found: with control CA clustering at high-perfusion/low-elastin and AD-HIES CA clustering at low-perfusion/high-elastin ends of the curve. Pearson correlation coefficient (r) is shown ($r = -0.82$; (95% CI: -0.96 to -0.41)). Such strong correlation suggests existence of coordinated interdependent regulation of these structural components of the vessel walls. Separation of AD-HIES and control CA on the curve suggests that this regulation is STAT3-dependent. Numbers next to each point show the patient age to demonstrate that there is no significant association with age (Adv perfusion vs Age: $r = -0.19$, $P = 0.6$; Adv elastin vs age: $r = 0.22$, $P = 0.5$).



Supplemental Figure 12 (related to Figure 7). Analysis of mouse model of AD-HIES.

(A-B) Structural abnormalities of coronary arteries in AD-HIES mouse model (additional images for Figure 7A-C). Coronary arteries were filled with solidifying silicone material (Figure 7A left panel) and CT scanning of the hearts was performed (see methods for details).

(A) Representative images of 3D reconstruction of coronary arterial network. Left Coronary Arteries (LCA) and its main branches of AD-HIES mice have higher degree of tortuosity.

(B) Examples of abnormalities detected in secondary branches of coronary arteries of AD-HIES mice: tortuosity, abnormal branching including backwards angles, multiple branching from one location. See also Figure 7A-C and Supplemental Movies 1 and 2.

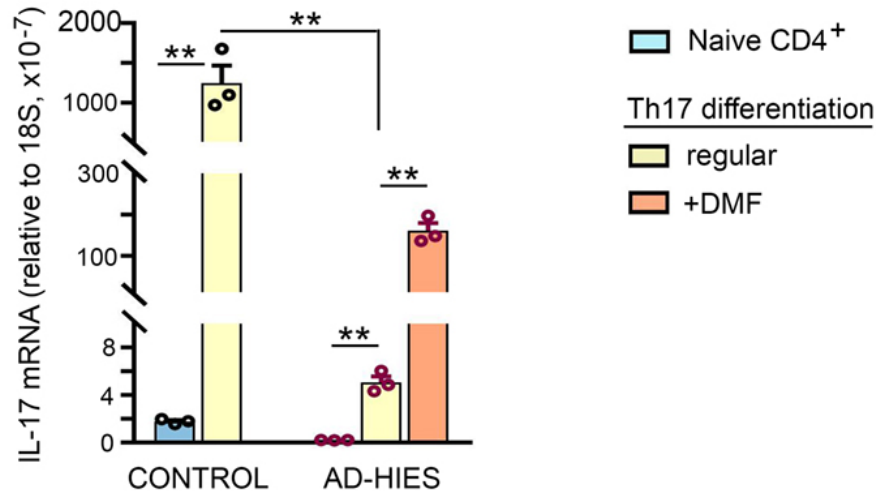
(C-E). Deficient skin wound healing in AD-HIES mice: additional information about wound healing model.

(C) Masson's stain of cross section of normal mouse skin. Mouse skin, unlike human, contains *panniculus carnosus* muscle and is not tightly attached to underneath skeletal muscles. Such anatomy results to wound closure primarily by contraction, while human wound healing occurs by re-epithelialization and granulation tissue formation.

(D, E) We used splinted wound healing model that minimizes contraction and promotes healing by re-epithelialization and granulation tissue formation and resemble human wound healing. See methods for details.

(D) Representative images of splinted wounds.

(E) Representative images of wound edges at day 4. WT mouse wound display more expanded granulation tissue (GT) filled with fibroblasts and immune cells and more advanced reepithelialization, consistent with faster wound closure shown on Figure 7H, 7I.



Supplemental Figure 13 (related to Figure 7). Dimethyl fumarate (DMF) improves Th17 generation from naïve cells of AD-HIES patients. 50,000 naïve CD4⁺ T cells from healthy controls and AD-HIES patients were subjected to Th17 differentiation procedure as described in Methods. IL-17 mRNA abundance was analyzed at the end of the differentiation as a measure of Th17 differentiation efficiency. Values shown are relative expression levels of triplicate samples (mean ± SEM, n=3, **P<0.01, two tailed unpaired t test) obtained from one control and one AD-HIES patient. Representative of 3 experiments performed on cells obtained from 3 controls and 3 AD-HIES patients is shown.

Supplemental Movies:

Supplemental Movie 1 (related to Figure 7). 3D reconstruction of coronary arterial network of AD-HIES mouse. To cast coronary arteries, they were filled with solidifying silicone material followed by CT scanning of the hearts. 3D reconstruction was performed using MATLAB software. *Red:* The Left Coronary Artery (LCA). *Yellow:* The Right Coronary Artery (RCA). *White:* The Septal Artery

Supplemental Movie 2 (related to Figure 7). 3D reconstruction of coronary arterial network of WT mouse. To cast coronary arteries, they were filled with solidifying silicone material followed by CT scanning of the hearts. 3D reconstruction was performed using MATLAB software. *Red:* The Left Coronary Artery (LCA). *Yellow:* The Right Coronary Artery (RCA). *White:* The Septal Artery

Supplemental Tables

Supplemental Table 1. Information about AD-HIES patients and controls used in the study.

See Excel file called "Supplemental Table 1"

- Sheet tab “AD-HIES & Control samples” : Provides demographic, genetic and clinical information about AD-HIES patients and information about tissues/cells used in the study
- Sheet tab “Patients used for each figure” : Provides information about patient samples and tissues that were used in experiments of the study: specified for each figure panel.

Supplemental Table 2 (related to Figure 2). RNA-Seq analysis of genes and signaling pathways that are affected by AD-HIES STAT3 mutations.

See Excel file called "Supplemental Table 2"

- Sheet tab “IFN-regulated & host defense” :
Table: IFN-regulated or host defense-related genes with increased expression in AD-HIES patient specific skin fibroblasts as compared to skin fibroblasts from normal volunteers.
Pathway map: Interferon-alpha/beta signaling via Jak/STAT pathway map showing genes that are differentially expressed in AD-HIES vs control skin fibroblasts
- Sheet tab “Cytokines & chemokines” :
Table: Abnormal expression patterns of cytokines and chemokines regulating inflammatory responses in AD-HIES patient specific skin fibroblasts as compared to skin fibroblasts from normal volunteers.
- Sheet tab “ECM & Growth factors” :
Table: Downregulated expression of genes related to extracellular matrix remodeling and growth factors signaling in AD-HIES patient specific skin fibroblasts as compared to skin fibroblasts from normal volunteers.
- Sheet tab “HIF1 α targets” :
Table: HIF1 α transcriptional targets with changed expression in AD-HIES skin fibroblasts as compared to fibroblasts from normal control volunteers.

Supplemental Table 3. Primer sequences that were used in the study.

| Gene | Forward primer | Reverse primer |
|----------------------------|------------------------|-------------------------|
| <i>ChIP primers</i> | | |
| <i>MMP1</i> | GGGTACCAGGCAGCTTAACA | TTGGAATCACTTGGTGTTGC |
| <i>MMP3</i> | AAGAACCAGCAAATCCAACG | CTCAACCTTCCCAATTTTGC |
| <i>MMP9</i> | CCATCAGAACCAGTCTTTTTCA | TGGCCTTTGTCTTCTTTCTCA |
| <i>KDR</i> | TGCTCCAGTTTTCTCCTCTACC | TTCATTTCCACTGGCTTTACTT |
| <i>HIF1A</i> | TTCCTTCGGAGAAGGCGCAG | TGTTTAGCGGCGGAGGAAAG |
| <i>qPCR primers</i> | | |
| <i>MMP1</i> | CCCTGAAGGTGATGAAGCAG | TGCTTGACCCTCAGAGACCT |
| <i>MMP3</i> | CCAATCCTACTGTTGCTGTG | GAGTGTCGGAGTCCAGCTTC |
| <i>MMP9</i> | CAGTCCACCCTTGTGCTCTT | GCCCTCAAAGGTTTGAATC |
| <i>KDR</i> | AGTGATCGGAAATGACACTGGA | GCACAAAGTGACACGTTGAGAT |
| <i>HIF1A</i> | GGCGCGAACGACAAGAAAAAG | CCTTATCAAGATGCGAACTCACA |
| <i>HIF2A</i> | CGGAGGTGTTCTATGAGCTGG | AGCTTGTGTGTTTCGCAGGAA |
| <i>VEGFA</i> | AGGGCAGAATCATCACGAAGT | AGGGTCTCGATTGGATGGCA |
| <i>FGF2</i> | AGAAGAGCGACCCTCACATCA | CGGTTAGCACACACTCCTTTG |
| <i>PLGF</i> | GAACGGCTCGTCAGAGGTG | ACAGTGCAGATTCTCATCGCC |

Supplemental methods

Page

(use links to page numbers and/or bookmarks for easier navigation)

| | |
|--|--------------------|
| Human wound healing model..... | 20 |
| Derivation of patient-specific skin fibroblasts..... | |
| Skin fibroblasts cell culture and treatments..... | |
| Derivation and culture of patient-specific Human Umbilical Vein Endothelial Cells (HUVEC) | |
| RNA-seq..... | 21 |
| Analysis of RNA-Seq data..... | |
| RNA extraction and quantification by real-time PCR..... | 22 |
| Western Blot..... | |
| Chromatin Immunoprecipitation (ChIP)..... | |
| STAT3 overexpression..... | 23 |
| shRNA knockdown..... | |
| siRNA knockdown..... | |
| HRE-luciferase reporter assay..... | |
| Measurement of angiogenic factors in cell culture supernatants..... | 24 |
| Endothelial cells tube formation assay..... | |
| Immunostaining of paraffin embedded tissue sections..... | |
| DAB intensity measurements on tissue sections..... | 25 |
| Mouse hind-limb ischemia model..... | |
| Treatment of mice with DMF by gavage..... | |
| IHC staining for CD31 with DAB visualization for assessment of capillary density..... | 26 |
| Analysis of coronary arteries abnormalities in AD-HIES mice..... | |
| Mouse wound healing model..... | 27 |
| Human coronary arteries..... | |
| Quantification of ECM proteins expression on sections of human coronary arteries..... | |
| Quantification of MMPs mRNA in sections of human coronary arteries..... | 28 |
| Quantification of the Vasa Vasorum (VV) on sections of human coronary arteries..... | |
| In vitro differentiation of naive CD4 ⁺ T cells from control and AD-HIES patients..... | |
| Teratoma formation from iPSCs and analysis of proportion of CD31 positive cells in the teratomas..... | |
| Immunostaining of teratomas sections for CD31..... | 29 |

Human wound healing model. After obtaining informed consent, skin biopsies for wound healing studies were collected under the NIAID IRB approved clinical trial NCT02262819. Skin wound was created using 2-mm skin punch biopsy tool. Three or seven days later 3-mm repeated skin punch biopsy of the wound site was taken and the wound healing process was analyzed by immunohistochemistry. The biopsies were fixed for 48 hours in 4% paraformaldehyde at 4°C, embedded in paraffin and sections were cut and mounted on positively charged slides. The sections were stained with antibodies as described in "Immunostaining of paraffin embedded tissue sections". The antibody used were: anti-HIF1 α (No.NB100-134; Novus Biologicals), EDTA retrieval; anti-P-STAT3 (Tyr705) (No.9145, Cell Signaling), EDTA retrieval; anti-STAT3 (No.9139, Cell Signaling) Citrate retrieval; anti- α -SMA (No.ab7817, Abcam), Citrate retrieval; anti-CD31 (No.M0823, DAKO), Citrate retrieval. Areas of granulation tissue for Figure 1B as well as cell numbers for Figure 1E were measured using Fiji ImageJ software. Integral intensity of DAB for HIF1 α and CD31 staining (Figures 1E and 5A) were measured as described in "DAB intensity measurements on tissue sections". For analysis presented on Figures 1E and 5A, 3-5 representative images were taken from each staining and then results obtained from each representative image were averaged to get final result for each staining.

Derivation of patient-specific skin fibroblasts. 3 Control and 3 AD-HIES patient-derived fibroblasts lines were generated from 3-4-mm skin biopsies following informed consent under protocols approved by NHLBI IRB. The skin biopsy was cut into 1mm pieces and digested for 1h at 37C in 10ml of 0.1% Collagenase Type II (No.17101-015, Thermo Fisher Scientific) / 0.25 U/ml Dispase (No. 17105-0411, Thermo Fisher Scientific)/PBS solution. The skin pieces were then transferred to 2 wells of a 6 well culture plate, covered with cover slips to facilitate attachment, and cultured in Dulbecco's modified Eagle medium (DMEM) supplemented with 20% fetal bovine serum and antibiotics in 20% O₂, 5% CO₂ incubator. Fibroblasts outgrown from the explants were subcultured after 3-4 weeks when they occupied most of the well's surface. The fibroblasts then were cultured in DMEM medium supplemented with 10% fetal bovine serum (No. S10250, Atlanta biological, Flowery Branch, GA) and antibiotics.

Skin fibroblasts cell culture and treatments. The fibroblasts were routinely grown in DMEM medium supplemented with 10% fetal bovine serum and seeded for experiments on six well plates at a density of 250,000 cells per well and switched to serum free medium after they reached confluence. After 24h in serum free medium, media was replaced with fresh serum free media and cells were treated in the experiment-specific manner as indicated in the figure legends. The following reagents were used for cell treatments: TNF α (No.300-01A, Peprotech, Rocky Hill, NJ); IL-6 (No.200-06, Peprotech, Rocky Hill, NJ); Dimethyl fumarate (DMF) (No.242926, Sigma), DMSO (No.4X, ATCC), DMOG (No.400091, EMD Millipore Corp), Cycloheximide (no.C7698, Sigma); Daprodustat (GSK1278863 (No.S8171, Selleckchem). For hypoxia exposure, the plates were transferred to a 1% O₂, 5% CO₂ incubator.

Derivation and culture of patient-specific Human Umbilical Vein Endothelial Cells (HUVEC). Informed consent from mothers was obtained for 3 patient and 2 control lines and one control line was purchased (No. PCS-100-010, ATCC). The cords were shipped overnight

from hospitals in PBS supplemented with Penicillin-Streptomycin (No. 15140122, ThermoFisher Scientific). Umbilical veins were washed 3 times with PBS supplemented with Penicillin-Streptomycin and Amphotericin B (No. 400-104, Gemini Bio-Products, West Sacramento, CA) and then filled with collagenase, type II (No.17101-015, ThermoFisher Scientific) at 0.2% in PBS and the ends were closed. The cords were placed in 37C incubator for 20 min. The cells were pelleted from the collagenase suspension, resuspended in endothelial cell culture media (EBM Basal Medium (No.CC-3121, Lonza) supplemented with EGM-2 SingleQuots Kit (No.CC-4176, Lonza)), Penicillin-Streptomycin and Amphotericin B and plated on fibronectin (No. F2006, Sigma) coated T25 flask. The media was changed next day, and cells were routinely cultured on 10 cm fibronectin coated dishes. For RNA isolation, HUVECs were seeded on 6 well plates at density of 250,000 cells per well. In 48 hours, when cells reached confluence, media was changed to fresh one with or without 50ng/ml TNF α for 8h and total RNA was extracted for RNA-Seq analysis.

RNA-seq. Total RNA was isolated using TRIzol Reagent (No. 15596026, ThermoFisher Scientific) for lysis and homogenization and isopropanol for precipitation. One μ g of total RNA was used as input for library preparation using the TruSeqRNA Sample Preparation Kit v2 (Illumina) according to manufacturer's instructions. Sequencing libraries were quantitated by qPCR on a LightCycler 480 Instrument II (Roche) and assessed for size distribution and absence of adapter dimers using a Fragment Analyzer (AATI). Libraries were pooled for multiplexing and sequencing was performed on the Illumina HiSeq 3000 Sequencing System with run parameters at paired-end 75bp read length for >25 million paired-end reads per sample.

Analysis of RNA-Seq data. RNA-seq data quality was assessed using FastQC (<http://www.bioinformatics.babraham.ac.uk/projects/fastqc/>) and all samples in this study passed quality control checks. Reads obtained for each sample were aligned to the hg19 human reference genome using Tophat2 (1) and read counts were generated using HTSeq (2). The statistical significance of differential expression (DE) were evaluated using DESeq2 (3) and edgeR (4). To identify sets of genes with shared function that were altered in AD-HIES patients derived skin fibroblasts and HUVECs, gene signature and pathway enrichment analysis were carried out using Gene Set Enrichment Analysis (GSEA) software from the Broad Institute (<http://software.broadinstitute.org/gsea/index.jsp>) (5), Pathway Studio software (Elsevier) and GeneGo MetaCore software (Thomson Reuters). The gene list of HIF1 α transcriptional targets (V\$HIF1_Q5) was obtained from the Molecular Signature Database (MSigDb, <http://software.broadinstitute.org/gsea/msigdb/index.jsp>) offered by GSEA. We also obtained a list of genes from Gene Ontology (<http://amigo.geneontology.org>) for the wound healing (GO: 0042060) and positive regulation of angiogenesis gene signatures (GO: 0045766). Clustering and heatmap visualization of gene expression patterns were done using the Genesis software (http://genome.tugraz.at/genesisclient/genesisclient_description.shtml) (6).

RNA extraction and quantification by real-time PCR. Total RNA was extracted from cultured cells using the RNeasy Mini Kit (Qiagen). The RNA (1 ug) was converted to cDNA by reverse transcription using TaqMan Reverse Transcription Reagents (N8080234; Applied Biosystems). mRNA levels were measured by real-time PCR using iQ SYBR Green Supermix (Bio-Rad) or QuantiFast SYBR Green PCR Kit (No. 204054, QIAGEN, Valencia, CA) on MJ Research Dyad Disciple thermal cycler with Chromo 4 fluorescence detector (Bio-Rad) or LightCycler 96 (Roche) Systems. Quantification was performed by the comparative CT method. 18S ribosomal RNA was used as an endogenous control. The relative copy number ($2^{-(Ct(\text{target mRNA}) - Ct(18S \text{ rRNA}))}$) of a target was calculated for each sample and normalized to the copy number in the corresponding control sample (the control samples are specified on figure legends).

Western Blot. Western analysis was performed by immunoblot of proteins separated by SDS-PAGE followed by chemiluminescent detection. Cultured cells were lysed with RIPA buffer (50 mM Tris-HCl, 1% NP-40, 0.5% Deoxycholate, 0.1% SDS, 150mM NaCl) supplemented with protease and phosphatase inhibitors. Sample loading onto gels was equalized according to the total protein concentration measured by BCA assay (N23225, Pierce, Rockford, IL). Primary antibodies were against p- STAT3 (Tyr705) (9145; Cell Signaling Technologies), STAT3 (9139; Cell Signaling Technologies), GAPDH (3683; Cell Signaling Technologies) and HIF1 α (#610959, BD Biosciences), α -tubulin (No.3873; Cell Signaling Technologies).

Chromatin Immunoprecipitation (ChIP).

1) ChIP for Supplemental Figure 5D was performed using EZChIP Kit (N17-371, EMD Millipore, Darmstadt, Germany). Briefly, skin fibroblasts grown on 15 cm dishes were cross linked with 1% formaldehyde for 10 min. The cells were lysed in SDS Lysis Buffer and the chromatin was sonicated to an average fragment size of approximately 500 bp. Fragmented chromatin from 1 million cells was pre-cleared with protein G Agarose beads and then immunoprecipitated with 2 μ g of anti- STAT3 (SC-482, SantaCruz Biotechnology) or with rabbit IgG. Cross-linking was reversed by overnight incubation at 65C and proteins in the samples were digested with Proteinase K. DNA was further purified using spin columns. The number of DNA fragments containing target sequences in the input chromatin and in the chromatin immunoprecipitated (IP) with anti- STAT3 and IgG were quantified by Real-Time PCR with iQ SYBR Green Supermix (Bio-Rad) on MJ Research Dyad Disciple thermal cycler with Chromo 4 fluorescence detector (Bio-Rad). STAT3 binding to the promoters of *MMPI*, *MMP3*, *MMP9* and *KDR* genes were quantified. The number of copies of each target sequence in STAT3 ChIP was normalized by the copy number in an IgG ChIP. See Supplemental Table 3 for the primers sequences.

2) ChIP for Figure 4D was performed using the Enzymatic Chromatin IP kit (No.9003, Cell Signaling Technology, Danvers, MA) according to the kit instructions. Briefly, cells were cross linked with 1% formaldehyde for 10 min. Chromatin was digested with MNase to generate fragments from 150bp to 900bp. For each sample, chromatin from 1 confluent 6 well plate was immunoprecipitated with 5 μ l of anti-Stat3 antibody (No. 9139, Cell Signaling Technology, Danvers, MA) or with mouse IgG (No.61656, Cell Signaling Technology, Danvers, MA).

Protein in samples was enzymatically digested, and the DNA was further purified. The number of DNA fragments containing target sequences in input chromatin and in chromatin immunoprecipitated (IP) with anti-Stat3 and IgG were quantified by QuantiFast SYBR Green PCR Kit (No. 204054, QIAGEN, Valencia, CA). STAT3 binding to target sequence in the promoter of *HIF1 α* gene were quantified. See Supplemental Table 3 and Supplemental Figure 9 for the primers information.

Quantification of STAT3 binding to promoters of analyzed genes was performed by Comparative CT method as fold increase of target fragments that were IPed by STAT3 antibody as compared to IgG. The relative to input DNA copy number of each target sequence for each IP sample was calculated as $2^{-(Ct(\text{IP DNA}) - Ct(\text{Input DNA}))}$. The number of copies of each target sequence in STAT3 ChIP was normalized by the copy number in an IgG ChIP.

STAT3 overexpression. Full length *STAT3* cDNA was purchased from Dharmacon (#7727). Using Invitrogen's Gateway Cloning System, the *STAT3* cDNA was subcloned to pLenti6.3/V5-DEST (Invitrogen, V53306). Virus was produced in HEK293FT cells using the ViraPower™ HiPerform™ Lentiviral Gateway Expression Kit (Invitrogen, K5330-00). Fibroblasts were virally transduced for 24-36 hours and screened for puromycin resistance to identify stably transfected cells. For experiments shown on Supplemental Figure 5B, lentiviral particles for overexpression of STAT3 protein (No. LVP383, GenTarget Inc, San Diego, CA) or GFP for control (No.LVP024, GenTarget Inc, San Diego, CA) were used. The fibroblasts were transduced for 48h before using for experiments.

shRNA knockdown. STAT3 and HIF1 α were knocked down with a human "GIPZ lentiviral shRNA" viral particle purchased from Dharmacon (RHS4531-NM_003150 and RHS4531-NM_001530). Fibroblasts were transduced for 24-36 hours and screened for puromycin resistance for stable transfections.

siRNA knockdown. Skin fibroblasts were transfected with 1:1 mixture of SignalSilence Stat3 siRNA I (No.6580, Cell Signaling) and SignalSilence Stat3 siRNA II (No. 6582, Cell Signaling) using Lipofectamine RNAiMAX reagent (No.13778150, ThermoFisher Scientific) according to the manufacture instructions. Reverse transfection protocol was used with 0.75ul of each siRNA and 1.5ul of RNAiMAX reagent per well of 24 well plate. The cells were used for the experiments after 36-48h.

HRE-luciferase reporter assay. The HRE-luciferase construct was a gift from Navdeep Chandel (Addgene plasmid # 26731) HRE-Luciferase is a pGL2 vector containing three hypoxia response elements from the *Pgk-1* gene upstream of firefly luciferase. Transfections were performed using the lipofectamine 2000 transfection reagent according to the manufacturer's protocol. (Thermofisher 11668027). After 48 hours, the media was replaced and cells were exposed to 1% O₂ or TNF α for the times indicated in the figure legends. Luciferase expression was measured by Promega's Dual-Luciferase® Reporter Assay System (E1910, Promega) using a 1450 MicroBeta JET Luminescence Counter (PerkinElmer, Shelton, CT).

Measurement of angiogenic factors in cell culture supernatants. Skin fibroblasts were incubated in serum free medium for 24h as described in the “cell culture and treatment” section and then the media was replaced with fresh serum free medium. Cell culture supernatants were collected after 7 hours for analysis. MMP1, MMP3, MMP9, FGF-1, FGF-2, PLGF, VEGFA were measured using a human magnetic Luminex Assay (R&D Systems Inc, Minneapolis, MN). The assay was performed according to the manufacturer’s instructions and measurements were done on a Luminex 100 System (Luminex, Austin, TX).

Endothelial cells tube formation assay. Cell culture supernatants were collected as described above. The tube formation assay was performed based on previously described protocols.(7) Human Umbilical Vein Endothelial Cells (HUVECs) (No. PCS-100-010, ATCC) (Figure 3C) or HUVECs isolated from AD-HIES patients or normal volunteers (Supplemental Figure 4E) were used for the assay. Growth Factor Reduced Basement Membrane Matrix (Matrigel) (No.354230, Corning) was used as substrate for the tube formation. HUVECs were routinely cultured in EBM Basal Medium (No.CC-3121, Lonza) supplemented with EGM-2 SingleQuots Kit containing 2% FBS, Hydrocortisone, hFGF-B, VEGF, R3-IGF-1, Ascorbic Acid, hEGF, GA-1000, Heparin (No.CC-4176, Lonza). Matrigel was added to wells of a 96 well plate (80ul/well) and kept in incubator for 30 min to allow it to solidify. For experiments shown on Figure 3C, HUVECs were trypsinized and resuspended in culture medium composed from 25% EBM Basal Medium (no growth factors added) and 75% of cell culture supernatants collected from control or AD-HIES skin fibroblasts. As a positive control, HUVECs were resuspended in regular endothelial cells growth medium fully supplemented with growth factors as described above. When needed, 50ng/ml VEGF-A (No.100-20, PeproTech, Rocky Hill, NJ) was added to the cell suspension. To neutralize VEGF-A, the cell culture medium was supplemented with 250ng/ml bevacizumab (No.A2006, Selleckchem, Houston, TX) and incubated for 30 min at 37C before preparing cell suspension. For experiments shown on Supplemental Figure 4E, the cells were resuspended in regular endothelial cells growth medium fully supplemented with growth factors. 100ul of the cell suspensions were added to the Matrigel containing wells and plate was returned to incubator. Images were taken using a Nikon Digital Sight DS-2MBWC camera and a Nikon TS100 Eclipse microscope (Figure 3C) or with ZEISS AxioCam 305 color camera and Axiovert A1 microscope (Figure 6F, Supplemental Figure 4E). For analysis, 3 phase contrast photographs of each well were taken and the images were automatically analyzed by NIH Image J 1.48v Program using the macro ‘Angiogenesis Analyzer’ by Gilles Carpentier (Gilles Carpentier. Contribution: Angiogenesis Analyzer, ImageJ News, 5 October 2012). We quantified junction formation, total tubule length, number of meshes formed and total mesh area. Quantification metrics of each well’s 3 photographs were averaged together for a “well average” before statistical analysis.

Immunostaining of paraffin embedded tissue sections. Sections were deparaffinized with xylene and rehydrated in a graded series of ethanol concentrations. Endogenous peroxidase was quenched by placing the slides in 3% hydrogen peroxide in methanol for 10 min. Heat-induced epitope retrieval was performed by boiling the slides for 6-10 min either in citrate retrieval solution, pH 6.0 (Invitrogen, Carlsbad, CA) or in EDTA retrieval solution (No.E1161, Sigma).

Slides were washed with PBS then stained with antibodies against protein of interest, using the Histostain-SP Kit (No. 95-9943, Invitrogen, Carlsbad, CA), according to the manufacturer's instructions. In brief, after exposure to serum blocking solution, the sections were incubated successively with primary antibody, biotinylated secondary antibody and streptavidin-HRP conjugate. Visualization was with diaminobenzidine (DAB) (No. D22187, Molecular Probes, Eugene, OR), which generates a brown-colored oxidation product upon reaction with the horseradish peroxidase (HRP) labeled streptavidin. Nuclei were stained with hematoxylin (blue). Pictures were taken with the Leica DMB4000 microscope using 40X objective

DAB intensity measurements on tissue sections. For quantification of the DAB intensity on tissue sections images throughout the study, we used the Yellow-CMYK channel method described by Pham *et al* (8). They demonstrated that images in the CMYK yellow channel correlate with the IHC DAB stain intensity. We extracted the CMYK yellow channel from the images of sections stained for proteins of interest with DAB (brown color) and with hematoxylin for nuclei (blue) (Supplemental Figure 11A) and quantified average yellow intensity per pixel as a measure of the proteins expression. We processed the images according to Pham *et al* (8), implementing with a Python script. The source image (R, G, B) was transformed to the final image (R', G', B') , as follows:

$$(R', G', B') = (Y, Y, 0)$$

$$\text{where } Y = 255 * \frac{(1-B)}{255-K} \text{ and } K = 255 - \max(R, G, B).$$

This transformation computes the yellow channel of the image by the RGB-to-CMYK format conversion and then loads that channel value back into the standard RGB image format. The effect of this transformation is to extract the yellow channel of the image. Examples of original images and images in the yellow channel after processing are given on Supplemental Figure 11A. The Python script that performs transformation described above is available upon request.

Mouse hind-limb ischemia model. 3-5 month old mice underwent right femoral artery ligation as previously described (9). The right femoral artery was ligated distal to the origin of the A. Profunda femoris. Injection of WT and AD-HIES fibroblasts was performed into right tibialis muscle 24 hours after arterial ligation (2mln cells in 100ul PBS per mouse). A Laser Doppler imager (MLDI 5063, Moor Instruments Ltd., Devon, UK) was used to estimate relative blood flow. Images were analyzed by moorLDI Software Version 5.3. Ligated over non- ligated ratios were calculated for each mouse and time point. For capillary density analysis, calf muscles were collected 3 weeks after femoral artery ligation.

Treatment of mice with DMF by gavage. DMF was dissolved in 0.08% Methocel/H₂O as vehicle and administered by oral gavage (15mg/kg body weight) twice a day as previously

described (10) starting 2 days before hind-limb ischemia surgery. For capillary density analysis, calf muscles were collected 4 weeks after femoral artery ligation.

IHC staining for CD31 with DAB visualization for assessment of capillary density. Mouse calf muscles were harvested after perfusion fixation of whole mice with 0.1% Glutaraldehyde/1.5% paraformaldehyde/PBS fixative. The muscles were further fixed for 48 hours in 4% paraformaldehyde at 4°C, embedded in paraffin and sections were cut and mounted on positively charged slides. The sections were stained with antibodies against CD31 (No. DIA 310, Dianova, Hamburg, Germany) as described in "Immunostaining of paraffin embedded tissue sections" using citrate buffer retrieval method. Number of capillaries was counted with Fiji ImageJ software (<https://imagej.net/Fiji>). For each mouse, the total number of capillaries was counted on 12 representative view fields of calf muscles sections from ligated and non-ligated hind-limbs. 3-5 mice were analyzed per each group. Results were expressed in number of capillaries per square millimeter.

Analysis of coronary arteries abnormalities in AD-HIES mice. *Casting and 3D reconstruction of coronary arteries network of mouse hearts.* Mice were heparinized and subsequently euthanized with CO₂. Anterior chest wall was removed and thoracic aorta cannulated with PE-10 tubing (Instech Laboratories, Inc, Plymouth Meeting, PA). Heart was then perfused with phosphate buffered saline containing sodium nitroprusside (Sigma-Aldrich, St. Louis, MO) followed by Microfil (Flowtech Inc, Carver, MA) mixed in a ratio of 800ul of Microfil, 100ul diluent, and 100ul curing agent. Microfil was allowed to solidify for 20 min, then heart was removed and placed in 10% buffered formalin (Figure 7A). The hearts were scanned at high resolution on a Quantum GX MicroCT Scanner (Perkin-Elmer, Hopkinton, MA). The x-ray source was set to a voltage of 90kV and current of 88uA. Raw data were obtained in a 36mm field of view (FOV) and an initial reconstructed voxel size (VOX) of 72um. Subvolume reconstructions were then generated in a more focused FOV (8-11mm) yielding a final VOX of 17-22um. DICOM images generated from the CT scan were then used for 3D reconstruction of coronary arteries network. Matlab VolumeViewer was used for visualizing left and right coronary arteries, segmented with threshold of intensity. *Quantitative analysis of tortuosity of left and right coronary arteries (LCA and RCA).* We used the medical imaging Analyze 12.0 (AnalyzeDirect, Overland, KS, USA) to import DICOM images obtained from the CT scan of mouse hearts. We then used the tree analysis tool within Analyze 12.0 to generate binary tree-like skeleton of the LCA and RCA with a threshold of intensity. We split the LCA and RCA into 2 separate skeletons from their branching points on the aorta. We then measured tortuosity between two or more adjacent branching points along tree-like skeleton on the primary LCA or RCA, and identified the most tortuous segment with maximal tortuosity for the LCA or RCA of a heart. We then compared the maximal tortuosity of LCA or RCA between WT and AD-HIES mice with t test. *Note: Tortuosity was calculated as the ratio of length of the path between 2 adjacent branching points over the Euclidean distance between the 2 points.*

Mouse wound healing model. Splinted mouse skin wound healing model was used (11, 12). Two 6-mm excisional wounds were created on back of each mouse with punch skin biopsy tool. Silicone splinting rings (No.GBLRD476687-20EA, Sigma) were attached with bonding adhesive (instant Krazy glue) and secured with 6 stitches. The wounds were covered with Tegaderm (3M) sterile transparent dressings that were changed every day during treatments (shown on Figure 7H and Supplemental Figure 12D). For topical treatments, dimethyl fumarate (DMF) (No.242926, Sigma) or daprodustat (GSK1278863) (No.S8171, Selleckchem) were dissolved in 5% polyethylene glycol (PEG) (PEG800 NF, No.SLP1393-500g, ScienceLab) at 1mM concentration and 30 μ l of the solutions were applied on the wounds once daily. Second wound on each mouse was treated with 5% PEG and served as no treatments control. 5% PEG8000 solution in water have been tested in this mouse wound healing model demonstrating no effect on wound healing rate (13). Images of the wounds were taken daily at time of treatment and dressing changing and the wound areas were measured with Fiji ImageJ software (<https://imagej.net/Fiji>) using inner splint hole as reference for the area calculations.

For IHC analysis of the wound healing process, additional series of the experiment were performed in which wounds were treated with DMF: skins were excised at day 4, fixed for 48 hours in 4% paraformaldehyde at 4°C, embedded in paraffin and sections were cut and mounted on positively charged slides. Immunostaining was performed as described in "Immunostaining of paraffin embedded tissue sections" section with anti-P-Stat3(Y705) (No.4113, Cell Signaling) (EDTA retrieval) and anti-HIF1 α (No. NB100-134, Novus Biologicals) (Citrate retrieval). For analysis of HIF1 α expression in granulation tissue (Figure 7L, 7M), 3-4 representative images were taken from each skin section. Integral intensity of DAB staining was measured on each image as described in "DAB intensity measurements" and cell number was counted using Fiji ImageJ. HIF1 α expression per cell was calculated by dividing total DAB intensity by cell number for each image and averaged for each mouse.

Human coronary arteries. Paraffin sections of control coronary arteries were obtained from CVPath Institute Inc, Gaithersburg MD. Sections of coronary arteries from 5 AD-HIES patients were obtained from National Cancer Institute Laboratory of Pathology, Bethesda, MD. Hematoxylin and eosin (H&E) and Movat pentachrome staining were performed by standard techniques by Pathology Core Facility of National Heart Lung and Blood Institute (Bethesda, MD).

Quantification of ECM proteins expression on sections of human coronary arteries. The sections were immunostained using DAB visualization as described in "Immunostaining of paraffin embedded tissue sections" with epitope retrieval methods modified depending on the antibody used. For Collagen I staining (anti-collagen I, No. GTX20292, Genetex, Irvine, CA), retrieval with citrate buffer was performed. For collagen IV (anti-collagen IV, No.GTX26586, Genetex) and elastin (anti-elastin, No. ab77804, Abcam, Cambridge, MA) citrate retrieval followed by 10 min incubation at 37C with ficin (No.003006, Invitrogen). For laminin (anti-laminin 1+2, No. GTX27463, Genetex), citrate retrieval followed by trypsin digestion for 10min at 37C (No.003006, Invitrogen).

To analyze the expression levels of the ECM proteins, we took 5 representative images from the adventitia, media, and intima of 3-8 control and 5 AD-HIES coronary arteries with the Leica DMB4000 microscope using a 40X objective. Intensity of DAB staining was measured on each image as described in "DAB intensity measurements on tissue sections" and averaged for all 5 representative images (see Supplemental Figure 11A). Results of the quantification are presented on Figure 5F.

Quantification of MMPs mRNA in sections of human coronary arteries. MMP1 and MMP3 mRNA were detected on formalin-fixed paraffin-embedded sections from control and AD-HIES coronary arteries by RNAscope Assay as previously described (14) using RNAscope 2.5 HD Reagent Kit – BROWN (Advanced Cell Diagnostics, Newark, CA). Representative images are shown on Figure 5C and Supplemental Figure 11B. 5 representative images were taken from each coronary artery with the Leica DMB4000 microscope using a 40X objective and number of spots was counted per μm^2 of adventitia (MMP1) or media (MMP3) as a measure of mRNA expression. The results were normalized to average spots density of control coronary arteries.

Quantification of the Vasa Vasorum (VV) on sections of human coronary arteries. Sections from 5 control and 5 AD-HIES coronary arteries were submitted for CD31 staining to PhenoPath Laboratories PLLC (Seattle, WA) to identify the Vasa vasorum (Figure 5D). Slides were scanned by NanoZoomer 2.0 RS slide scanner (Hamamatsu Photonics) and images were analyzed with the NDP.view2 software (Hamamatsu Photonics). The total number of VV vessels with a diameter larger than 10 μm were counted in the adventitia of the coronary arteries and the perimeter of each VV vessel was measured. The density of the VV was calculated as the number of vessels per mm^2 of the adventitia area. The cross sectional area of each VV vessel was calculated from its perimeter. For each coronary artery, adventitial blood perfusion was estimated as % of adventitia occupied by blood vessels: $(\text{Area}_{\text{VV}} / \text{Area}_{\text{Adv}}) \times 100$.

***In vitro* differentiation of naïve CD4⁺ T cells from control and AD-HIES patients.**

Differentiation of naïve CD4⁺ T cells to Th17 cells and IL-17 mRNA qPCR analysis were performed as previously described(15). Briefly, naïve CD4⁺ T cells were purified from peripheral blood by magnetic cell sorting with a human naïve CD4⁺ T-cell isolation kit (Miltenyi Biotec). The cells were plated on 96 well plate in Th17 differentiation conditions for 12 days. For dimethyl fumarate (DMF) treatment, DMF was added to Th17 differentiation medium at concentration 5 μM . RNA was isolated using RNeasy Mini Kit (Qiagen), converted to cDNA by reverse transcription using TaqMan Reverse Transcription Reagents (Applied Biosystems). TaqMan primers and probes for human IL-17 mRNA were purchased from Applied Biosystems. Expression level was analyzed with the ABI Prism 7500 Fast Real-Time PCR System (Applied Biosystems). The expression is calculated as copy number relative to 18S rRNA ($(2^{-\text{Ct}(\text{IL-17 mRNA})} - \text{Ct}(18\text{S rRNA}))$).

Teratoma formation from iPSCs and analysis of proportion of CD31 positive cells in the teratomas. iPSCs were generated from Control and AD-HIES skin fibroblasts as previously described (16). Non-obese diabetic (NOD) severe combined immunodeficiency (SCID) gamma (NSG) mice (Jackson Laboratory, Bar Harbor, ME) were used for the teratoma assay. For

teratoma formation, 3–5 x 10⁶ iPSCs or 1:1 mixture of iPSCs with fibroblasts were suspended in 30% Basement Membrane Matrix, High Concentration, LDEV-free solution (BD Biosciences) and subcutaneously injected into the hindlimbs of NSG mice. Teratomas formed within 8 weeks and were excised for analysis (17). Teratomas were digested using the Liberase TL Research Grade Enzyme Blend (No.05401020001, Roche Applied Science, Mannheim, Germany) based on the manufacture instruction. Briefly, teratomas were cut into small pieces and incubated in 200 µg/ml of Liberase-TL digestion solution for 10 min at 37C. The cells were stained with anti-human CD31 antibodies (No.303116, BioLegend, San Diego, CA) or with anti-human CD45 (No.304012, BioLegend, San Diego, CA). Analysis was performed on a BD FACSCanto Flow Cytometer (BD Bioscience, San Jose, CA) and the results were analyzed using FlowJo software (FlowJo, LLC). See Supplemental Figure 7B for the gating strategy.

Immunostaining of teratomas sections for CD31. The sections were stained with mixture of two antibodies against CD31 (No. DIA 310, Dianova, Hamburg, Germany and No.M0823, DAKO) as described in "Immunostaining of paraffin embedded tissue sections" using citrate followed by EDTA buffers retrieval methods.

References

1. Kim D, Pertea G, Trapnell C, Pimentel H, Kelley R, and Salzberg SL. TopHat2: accurate alignment of transcriptomes in the presence of insertions, deletions and gene fusions. *Genome Biol.* 2013;14(4):R36.
2. Anders S, Pyl PT, and Huber W. HTSeq--a Python framework to work with high-throughput sequencing data. *Bioinformatics.* 2015;31(2):166-9.
3. Love MI, Huber W, and Anders S. Moderated estimation of fold change and dispersion for RNA-seq data with DESeq2. *Genome Biol.* 2014;15(12):550.
4. Robinson MD, McCarthy DJ, and Smyth GK. edgeR: a Bioconductor package for differential expression analysis of digital gene expression data. *Bioinformatics.* 2010;26(1):139-40.
5. Subramanian A, Tamayo P, Mootha VK, Mukherjee S, Ebert BL, Gillette MA, et al. Gene set enrichment analysis: a knowledge-based approach for interpreting genome-wide expression profiles. *Proc Natl Acad Sci U S A.* 2005;102(43):15545-50.
6. Sturn A, Quackenbush J, and Trajanoski Z. Genesis: cluster analysis of microarray data. *Bioinformatics.* 2002;18(1):207-8.
7. Arnaoutova I, and Kleinman HK. In vitro angiogenesis: endothelial cell tube formation on gelled basement membrane extract. *Nature Protocols.* 2010;5(4):628-35.
8. Pham N-A, Morrison A, Schwock J, Aviel-Ronen S, Iakovlev V, Tsao M-S, et al. Quantitative image analysis of immunohistochemical stains using a CMYK color model. *Diagnostic Pathology.* 2007;2.
9. Limbourg A, Korff T, Napp LC, Schaper W, Drexler H, and Limbourg FP. Evaluation of postnatal arteriogenesis and angiogenesis in a mouse model of hind-limb ischemia. *Nature Protocols.* 2009;4(12):1737-48.
10. Schilling S, Goelz S, Linker R, Luehder F, and Gold R. Fumaric acid esters are effective in chronic experimental autoimmune encephalomyelitis and suppress macrophage infiltration. *Clinical and Experimental Immunology.* 2006;145(1):101-7.
11. Wang XS, Ge JF, Tredget EE, and Wu YJ. The mouse excisional wound splinting model, including applications for stem cell transplantation. *Nature Protocols.* 2013;8(2):302-9.
12. Galiano RD, Michaels J, Dobryansky M, Levine JP, and Gurtner GC. Quantitative and reproducible murine model of excisional wound healing. *Wound Repair and Regeneration.* 2004;12(4):485-92.
13. Park SA, Teixeira LBC, Raghunathan VK, Covert J, Dubielzig RR, Isseroff RR, et al. Full-thickness splinted skin wound healing models in db/db and heterozygous mice: Implications for wound healing impairment. *Wound Repair and Regeneration.* 2014;22(3):368-80.
14. Wang F, Flanagan J, Su N, Wang LC, Bui S, Nielson A, et al. RNAscope A Novel in Situ RNA Analysis Platform for Formalin-Fixed, Paraffin-Embedded Tissues. *Journal of Molecular Diagnostics.* 2012;14(1):22-9.

15. Milner JD, Brenchley JM, Laurence A, Freeman AF, Hill BJ, Elias KM, et al. Impaired T(H)17 cell differentiation in subjects with autosomal dominant hyper-IgE syndrome. *Nature*. 2008;452(7188):773-U11.
16. Jin H, Yu Z, Navarengom K, Liu YTY, Dmitrieva N, Hsu AP, et al. Generation of human induced pluripotent stem cell lines (NIHTVBi011-A, NIHTVBi012-A, NIHTVBi013-A) from autosomal dominant Hyper IgE syndrome (AD-HIES) patients carrying STAT3 mutation. *Stem Cell Research*. 2019;41.
17. Jin H, St Hilaire C, Huang YT, Yang D, Dmitrieva NI, Negro A, et al. Increased activity of TNAP compensates for reduced adenosine production and promotes ectopic calcification in the genetic disease ACDC. *Science Signaling*. 2016;9(458).